

Alkaline Earth Metal Ion Induced Coil–Helix–Coil Transition of Lysine–Coumarin–Azacrown Hybrid Foldamers with OFF–OFF–ON Fluorescence Switching

Yu-Chen Lin and Chao-Tsen Chen*^[a]

Abstract: A new metal-ion-responsive and fluorescent foldamer, **OPLM**₈, composed of eight lysine–coumarin–azacrown units, has been designed and synthesized. The flexible **OPLM**₈ can be forced into a well-defined helix structure only upon the addition of alkaline earth metal ions. The structural change is based on the crown ether moieties being positioned in the requisite arrangement along the peptide chain, that is, at *i*, *i*+4 spacing, such that the alkaline earth metal ions can mediate the formation of four sandwich complexes between them. Moreover, varying the chelator-to-metal-ion ratio from 2:1 to 1:1 resulted in disassembly of the sandwich complexes leading to collapse of the helical struc-

ture to a random coil. These metal-ion-induced structural transitions could not only be monitored by the CD amplitude change but also easily probed by unique “OFF–OFF–ON” fluorescence intensity changes from 0.7-fold to 14-fold as the structure changed from the folded helix to a random coil. To further verify that the helix formation was indeed induced by metal-ion complexation, two kinds of control octamers with only four metal-ion chelators on the side chains were studied. One, which was capable of forming two

sandwich complexes between the *i* and *i*+4 residues, displayed a negative Cotton couplet with the magnitude of its *A* value close to half that of **OPLM**₈, and the second had four metal-ion chelators positioned in the same turn, and hence was incapable of forming intramolecular metal complexes and showed different induced CD signals. Collectively, the photospectroscopic data and the results of the control studies suggest that alkaline earth metal ions can efficiently promote the flexible octamer **OPLM**₈ into a well-organized helix by the formation of sandwich complexes between substituents at an *i*, *i*+4 spacing.

Keywords: fluorescence • foldamers • helical induction • metal ions • sandwich complexes

Introduction

The helix is one of the essential structural elements in nature. Important biopolymers such as polypeptides and proteins fold and self-assemble into these unique and hierarchical structures, which play important roles in biocatalytic functions, gene transcription, protein aggregation, and disease treatments.^[1] The design of artificial helical structures that closely mimic native helices can help to elucidate key features of the structure and function of these helices, and also allows the introduction of novel biological and chemical reactivity into the relevant architectures. For example, synthetic helical molecules have displayed great potential for applications in chiral catalysts, chiral sensors, chiro-optical switches, and chiral-based information storage.^[2] Among these molecules, polymers that fold into a helical form in response to external stimuli are of particular interest.

Functional groups capable of non-covalent or covalent interactions, such as van der Waals, hydrophobic, hydrogen-bonding, and electrostatic interactions, and metal-ion-coordination interactions of varying strengths, are often judiciously incorporated into either the backbones or side chains of these molecules to facilitate the formation of helical structures. Thus, anion-responsive foldamers,^[3] composed of aryl strand building blocks with hydrogen-bond donors or polar C–H bonds, such as indolecarbazole^[4] or aryl-1,2,3-triazole,^[5] were found to fold into stable helical conformations upon the binding of complementary anions. Metal-ion-induced foldamers have been constructed from heterocycles^[6] such as pyrimidine–pyridine oligomers or a pyridine–oxazole framework,^[7] which provided coordination bonds to form single- or double-stranded helicates in the presence of suitable metal ions. Peptidomimetic foldamers derived from natural or unnatural amino acids have also been shown to adopt stable helical structures through the introduction of side-chain interactions in the regular spatial arrangement.^[8] In this context, Fujita et al. have demonstrated that aromatic–aromatic interactions between aromatic amino acid residues and electron-deficient triazine units of a host cage promoted the formation of short oligopeptides adopting a stable helix.^[9] Among them, foldamers that were mediated by stronger interactions displayed higher stability.

[a] Dr. Y.-C. Lin, Prof. Dr. C.-T. Chen
Department of Chemistry, National Taiwan University
No. 1, Sec. 4, Roosevelt Road, Taipei, 10617 Taiwan (R.O.C.)
Fax: (+886)2-23636359
E-mail: chenct@ntu.edu.tw

Supporting information for this article is available on the WWW under <http://dx.doi.org/10.1002/chem.201202998>.

The helicity induced in the foldamers is typically probed by circular dichroism, whereas fluorescence is more suitable for monitoring the folding–unfolding transition as it provides highly sensitive detection, environmental sensitivity, and real-time detection characteristics, thus allowing the detection of minimal conformational changes.^[10] However, synthetic foldamers equipped with suitable fluorophores sensitive to conformational changes have seldom been reported in the literature. Only a few examples utilizing Förster resonance energy transfer, fluorescence quenching by electron transfer, or excimer formation as sensing mechanisms^[11] have hitherto been demonstrated. In our previous study, we developed a highly selective fluorescent chemosensor (**DEAC**, Figure 1) that consisted of a [15]azacrown-5 ether

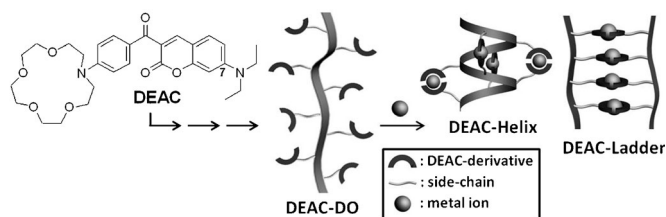


Figure 1. Schematic representation of highly ordered suprastructures induced by sandwich complexes between **DEAC-DO** and metal ions.

(ionophore) and a ketoaminocoumarin (fluorophore).^[12] This molecular sensor showed a high affinity for the toxic metal-ion Pb^{2+} through the formation of a 2:2 complex involving coordination of the carbonyl groups present in the fluorophore and ionophore moieties, which was accompanied by the emission of fluorescence. Inspired by these complexation features, we envisaged that an oligomer **DEAC-DO**, constructed from a **DEAC**-derivatized monomer, could possibly organize itself into the intramolecular helix-folded **DEAC-Helix** and/or the intermolecular-ladder-like **DEAC-Ladder** forms upon the complexation of appropriate metal ions (Figure 1). At the same time, these conformational

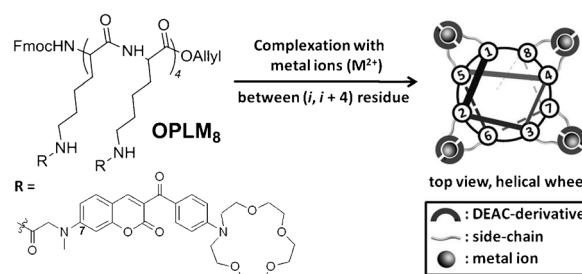


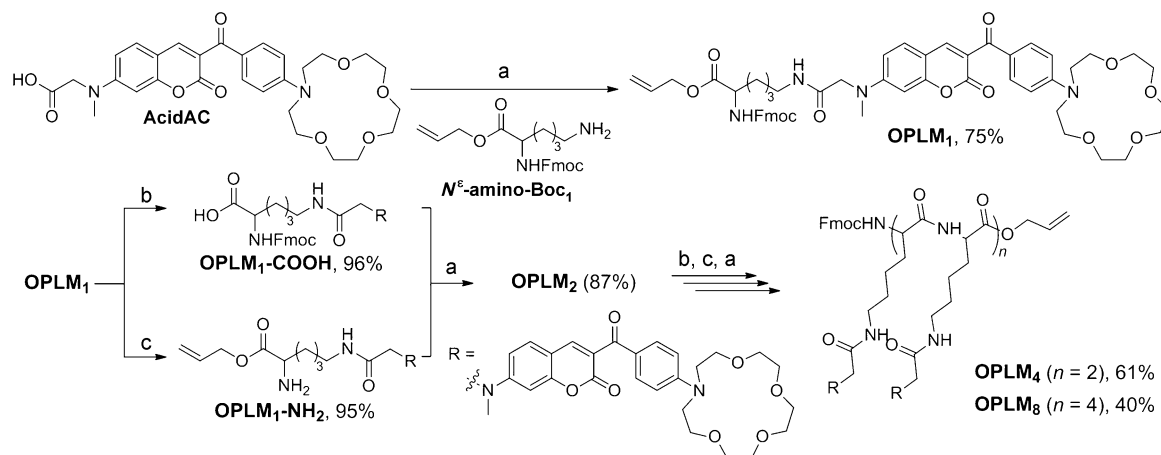
Figure 2. Chemical structure of the synthetic foldamer **OPLM₈** and a helical wheel representation of the **OPLM₈·4M²⁺** complex, which results from metal-ion-assisted folding of **OPLM₈**.

transitions (folding/unfolding) would be observable through fluorescence changes. Moreover, the ketocoumarin fluorophores, having favorable visible absorptions, would allow monitoring of the extent of the helicity by circular dichroism in the visible spectral region.

A metal-ion-responsive and fluorescence-detectable foldamer, **OPLM₈**, was thus designed and synthesized (Figure 2). **OPLM₈** comprises of eight **DEAC**–lysine hybrid residues. An oligo-L-lysine backbone was chosen because it can be easily functionalized on the side-chain N^ϵ -amino group through amide bond linkages. **OPLM₈** could potentially fold into a helical structure upon complexation with metal ions capable of promoting the formation of intramolecular sandwich complexes between the **DEAC** side chains at the i and $i+4$ positions. A helical wheel representation of the **OPLM₈·4M²⁺** complex is shown in Figure 2.

Results and Discussion

Synthesis of OPLM₈: **OPLM₈** was prepared by a solution-phase synthesis^[13] involving successive amide couplings of **OPLM₁**, **OPLM₂** (dimer of **OPLM₁**), and **OPLM₄** (tetramer of **OPLM₁**), as shown in Scheme 1. The starting building



Scheme 1. Synthesis of **OPLM₈**. Reagents and conditions: a) DCC, DMAP, HOBt, CH_2Cl_2 , RT, 12–36 h; b) $[\text{Pd}(\text{PPh}_3)_4]$ (10 mol %), *N*-methylaniline, CH_2Cl_2 , RT, 2–6 h; c) piperidine (20 %)/DMF, RT, 10–30 min.

block, **OPLM**₁, was first obtained from a **DEAC** derivative with an *N*-methyl-*N*-glycine moiety at the C-7 position (**AcidAC**) and an Fmoc/allyl-protected lysine residue (**N^ε-amino-Boc**) by an amide coupling promoted by *N,N*-dicyclohexyl carbodiimide (DCC) and hydroxybenzotriazole (HOBt) according to known procedures.^[13] Once the **OPLM**₁ monomer had been prepared, **OPLM**₂, **OPLM**₄, and **OPLM**₈ were subsequently obtained by iterative synthetic steps involving selective deprotection of the allyl ester and Fmoc groups (to provide the corresponding carboxyl- and amino-terminal functional groups) followed by amide coupling. Selective deprotections of the allyl and Fmoc groups were achieved in high yields by using a palladium catalyst (e.g., [Pd(PPh₃)₄]) and piperidine/dimethylformamide (DMF) solution (20%), respectively. The amide couplings were then carried out as described for **OPLM**₁. Detailed synthetic procedures and structural characterizations can be found in the Supporting Information.^[14]

Photospectroscopic properties of OPLM_n (n=1, 2, 4, 8) in the absence and presence of metal ions: The photospectroscopic features of **OPLM_n** (*n*=1, 2, 4, 8) in CH₂Cl₂ solution

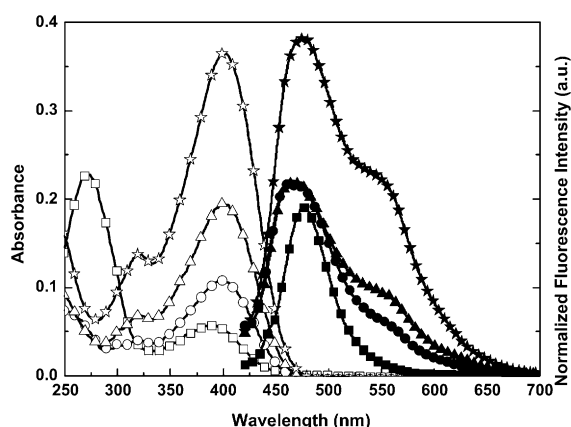


Figure 3. UV/Vis (open symbols) and normalized fluorescence emission spectra (solid symbols) of **OPLM_n** (*n*=1, 2, 4, 8; 10⁻⁶M) in CH₂Cl₂ (**OPLM**₁: λ_{exc}=388 nm; **OPLM_n**: λ_{exc}=400 nm). **OPLM**₁ (■), **OPLM**₂ (●), **OPLM**₄ (▲), **OPLM**₈ (★).

were studied by UV/Vis and fluorescence spectroscopies (Figure 3). In contrast to the distinct fluorescence emission spectra, the dimer, tetramer, and octamers of **OPLM**₁ exhibited very similar UV/Vis absorption profiles, albeit with slightly red-shifted wavelengths. The fluorescence emission spectra showed, besides the emission peak corresponding to the ketocoumarin moiety at 475 nm, a broad peak at around 550 nm that gradually intensified as the number of ketocoumarin groups was increased. This emission peak is attributed to the structural rigidity of the oligo(L-lysine) backbone in **OPLM_n**, which restricts the segmental mobility as a result of a certain degree of side chain–side chain interactions between coumarin moieties.

Although **DEAC**, which constitutes the designated metal-ion chelating site of **OPLM**, has been demonstrated to have high specificity for Pb²⁺ ion,^[12] it could display different metal-ion specificity once incorporated into the oligomer, because its disposition may no longer be optimal for forming the same Pb²⁺ complexes as observed in solution. With the aim of evaluating which metal ions are capable of forming complexes with **OPLM**₈, 17 metal ions (Li⁺, Na⁺, K⁺, Mg²⁺, Ca²⁺, Sr²⁺, Ba²⁺, Mn²⁺, Fe²⁺, Co²⁺, Ni²⁺, Cu²⁺, Ag⁺, Zn²⁺, Cd²⁺, Hg²⁺, and Pb²⁺, with perchlorate as the counter ions) were investigated by high-throughput fluorescence screening in CH₂Cl₂ (Figure S3 in the Supporting Information). The results indicated that **OPLM**₈ does indeed display different metal-ion specificities. Upon the addition of seven of these metal ions, namely Na⁺, K⁺, Ag⁺, Ca²⁺, Sr²⁺, Ba²⁺, and Zn²⁺, **OPLM**₈ exhibited noticeable fluorescence changes that were not observed with the other metal ions.

Although the high-throughput results provided an initial screening of potential candidates for inducing a conformational change in **OPLM**₈, more detailed follow-up studies of the influential metal ions were required to understand the relationship between optical properties and metal-ion-binding modes. The absorption and emission spectra of **OPLM**₈ in the presence of 4 and 10 equivalents of each of the influential metal ions (Na⁺, K⁺, Ag⁺, Ca²⁺, Sr²⁺, Ba²⁺, and Zn²⁺) were recorded and the results can be found in the Supporting Information (Figure S4 and Table S1). Based on

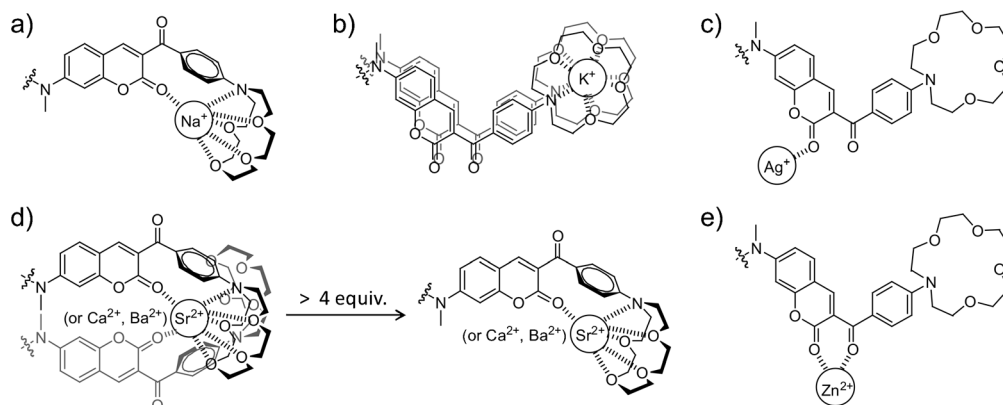


Figure 4. Proposed binding modes of **DEAC** derivatives to metal ions a) Na⁺, b) K⁺, c) Ag⁺, d) Ca²⁺, Sr²⁺, Ba²⁺, and e) Zn²⁺.

the observed spectral changes, several complexation modes could be proposed for the various metal ions (Figure 4). For example, the addition of Na^+ to **OPLM₈** gave rise to a sharp emission band at 485 nm with 13-fold enhancement (Figure S4a in the Supporting Information), as well as a moderate red-shift in the absorption spectrum by about 20 nm, indicating that the carbonyl from chromen-2-one moiety and the [15]azacrown-5 cavity of the **DEAC** derivative took part in the chelation (Figure 4a).^[12] In the case of K^+ , there was no appreciable change in the absorption, but a 1-fold fluorescence enhancement with a shoulder at 550 nm, suggesting that two azacrown moieties of **DEAC** sandwiched one K^+ ion. The K^+ cation is 40% larger than the Na^+ ion and cannot be accommodated well in the azacrown cavity; rather, it is known to form a sandwich complex with two [15]azacrown-5 ether moieties (Figure 4b).^[15] This complexation mode drew two coumarin moieties close together, resulting in fluorescence at 550 nm (Figure S4b in the Supporting Information). The addition of Ag^+ to **OPLM₈** yielded relatively small red-shifts in the absorption (ca. 11 nm) and fluorescence quenching, suggesting that only the carbonyl groups of the **DEAC** derivative coordinated to Ag^+ (Figure 4c and Figure S4c in the Supporting Information). In contrast, upon the addition of divalent metal ions such as Ca^{2+} , Sr^{2+} , and Ba^{2+} to **OPLM₈**, pronounced bathochromic shifts in the absorption in the range 30–40 nm were generally observed. However, the addition of Zn^{2+} ions gave the largest red-shift (ca. 62 nm), suggesting the establishment of a strongly stabilized internal charge-transfer (ICT) state upon complexation of Zn^{2+} ions with the two carbonyl groups of the **DEAC** derivative (Figure 4e).^[12] While the fluorescence intensity was almost quenched in the presence of Zn^{2+} ions (Figure S4g in the Supporting Information), a unique fluorescence intensity change pattern (OFF–OFF–ON)^[16] between 4 and 10 equivalents of Ca^{2+} , Sr^{2+} , or Ba^{2+} was observed, indicating that these cations must bind differently to Zn^{2+} . The emission spectra recorded in the presence of Ca^{2+} , Sr^{2+} , and Ba^{2+} ions showed a peak near 500 nm and a broad shoulder at around 550–600 nm, strongly suggesting that the **DEAC** derivative moieties were aggregated to a significant extent upon the addition of 4 equivalents of these metal ions (Figure 4d and Figure S4d–f in the Supporting Information).

To further clarify which metal ions could induce the hel-

ical suprastructure, changes in the circular dichroism signals of **OPLM₈** before and after addition of the influential metal ions were examined (Figure S5 and Table S1 in the Supporting Information). The results showed that only the addition of Ca^{2+} , Sr^{2+} , and Ba^{2+} resulted in a net induced circular dichroism (ICD) response with negative signs of the exciton Cotton effects, with no such effect being observed with Na^+ , Ag^+ , K^+ , or Zn^{2+} . The findings indicate that Ca^{2+} , Sr^{2+} , and Ba^{2+} , having appropriate sizes, suitable surface charge densities, and preferred coordination geometries,^[17] effectively cross-link two **DEAC** units via the azacrown and carbonyl groups, leading to the formation of a helical suprastructure, whereas Na^+ , Ag^+ , K^+ , and Zn^{2+} are not suitable mediators for the folding of **OPLM₈** into helical structures.

Titration of **OPLM₈** with Sr^{2+} ions to delineate the folding process:

The addition of Sr^{2+} resulted in the most pronounced change in the circular dichroism spectrum (Figure S5e in the Supporting Information) among the alkaline earth metal ions that were investigated, thus titrations of foldamer **OPLM₈**, **OPLM₂**, and **OPLM₄** with various amounts of Sr^{2+} were performed (Figure 5 and Figures S6–S8 in the Supporting Information) to delineate how the folding transition process of **OPLM₈** was influenced by an increasing amount of alkaline earth metal ions. The correlation of absorption intensity changes and number of metal-ion equivalents (absorption isotherm, black squares in the inset of Figure 5a) showed that saturation was reached upon the addition of 4 equivalents of Sr^{2+} ions. The fluorescence isotherm (gray circles in the inset) showed significant fluo-

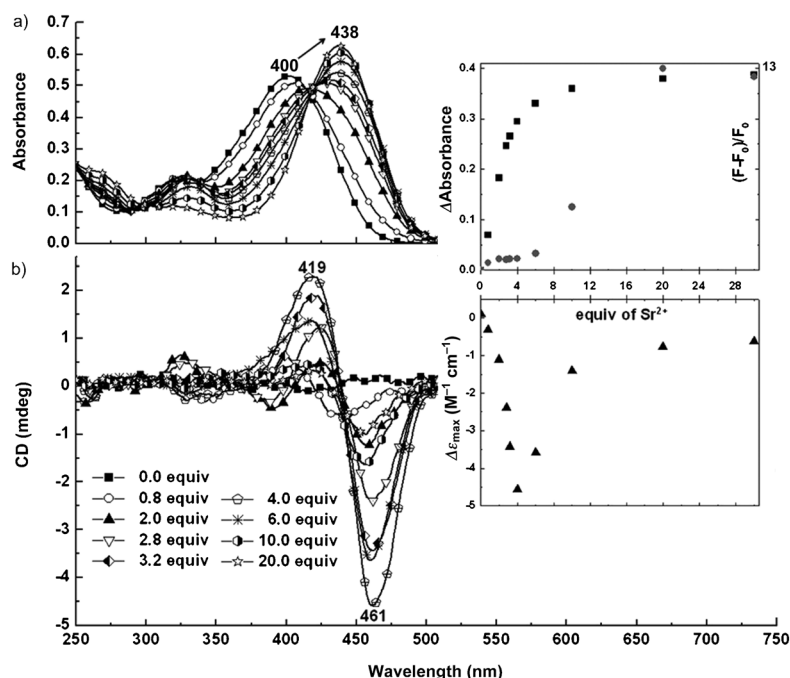


Figure 5. a) Overlaid absorption spectra of **OPLM₈** ($2 \times 10^{-6} \text{ M}$ in CH_2Cl_2) and b) the corresponding overlaid CD spectra upon the addition of increasing amounts of Sr^{2+} . Insets show the correlation of the absorbance wavelength changes (■) at 438 nm and fluorescence intensity changes (●), and ICD signal changes (▲) at 461 nm, with the amount of $\text{Sr}(\text{ClO}_4)_2$.

rescence quenching upon the addition of less than 4 equivalents of Sr^{2+} , while further fluorescence enhancement was observed at higher amounts of Sr^{2+} . The CD titration spectra^[18] exhibited zero CD signal in the absence of Sr^{2+} . As the amount of Sr^{2+} was increased up to 4 equivalents (Figure 5b and inset therein), an intense ICD signal with negative first and positive second Cotton effects at 461 and 419 nm, respectively, was observed. However, at higher Sr^{2+} content (more than 4 equivalents), the amplitude of the ICD signals decreased, indicating structural changes. It is worth noting that the zero-crossing point of the ICD signal at 438 nm corresponded well to the absorption spectral region of the Sr^{2+} -azacrown-coumarin complex.

In the case of **OPLM₂**, saturation was reached upon the addition of 2 equivalents of Sr^{2+} ions, with a large fluorescence enhancement (Figure S7 in the Supporting Information). The fluorescence titration profile appeared very different from that of **OPLM₈** titrated with Sr^{2+} , suggesting a different binding mode. Moreover, no ICD signal was observed in the presence of various amounts of Sr^{2+} (Figure S9a in the Supporting Information), reflecting the fact that the dipeptide is too short to fold into any form of secondary structure even with the aid of strong metal-ion coordination. When the tetramer **OPLM₄** was titrated with Sr^{2+} , three phases of fluorescence changes were observed. On the addition of up to 2 equivalents of Sr^{2+} , only a small fluorescence intensity increment was observed. However, the fluorescence at 500 nm increased rapidly when more Sr^{2+} was added, and reached saturation at 4 equivalents of Sr^{2+} . The subsequent addition of more Sr^{2+} resulted in a decrease in the intensity at 500 nm accompanied by the emergence of an emission band at 550 nm (Figure S8 in the Supporting Information). The corresponding CD titration spectra showed that the ICD signals were split into negative peaks at 460 and 338 nm and a positive peak at 409 nm in the presence of 0.4–2.4 equivalents of Sr^{2+} and that further addition of Sr^{2+} resulted in sharply diminished signals at 338 and 409 nm as well as a blue shift of the signal at 460 nm to 430 nm (Figure S9b in the Supporting Information). These observations indicated that the tetramer was quite flexible and could assume various secondary structures under the influence of different amounts of Sr^{2+} . In comparison with **OPLM₄**, **OPLM₈** displayed consistent changes in its absorption, fluorescence, and CD spectra when titrated with Sr^{2+} , suggesting that the structural transitions were more meaningful, and thus further investigations were focused on **OPLM₈**.

Proposed metal-ion-induced structural transition of **OPLM₈**:

Based on the titration results, a model for the Sr^{2+} -ion-induced conformational transition of **OPLM₈** was proposed (Figure 6). In the presence of 4 equivalents of side-chain cross-linking agent (e.g., Ca^{2+} , Sr^{2+} , or Ba^{2+}), four sandwich complexes formed between the **DEAC** moieties and induced **OPLM₈** to fold into a left-handed helix along the oligomer backbone, and the ICD intensity reached

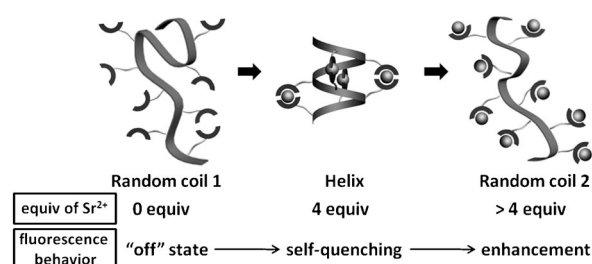


Figure 6. Graphical illustration of conformational transition of **OPLM₈** in the absence and presence of various equivalents of Sr^{2+} ions.

a maximum in the presence of 4 equivalents of metal ions. No obvious fluorescence changes appeared, a result of the close spatial proximity of the fluorophores (**Helix**, fluorescence self-quenching state, Figure 6). Upon the addition of larger amounts of Sr^{2+} ions, the variation of the chelator-to-metal ratio from 2:1 to 1:1 resulted in dissolution of the sandwich complexes, leading to collapse of the helical structure (**Random coil 2**, as shown in Figure 6). Accordingly, the CD intensity gradually decreased with a concomitant fluorescence increase caused by gradual separation of the fluorophores. The fluorescence OFF–OFF–ON changes and the selectivity of the metal-ion-induced folding/unfolding transition of **OPLM₈** corroborated the preliminary results of high-throughput fluorescence screening, thereby suggesting that alkaline earth metal ion induced structural transitions could be easily followed by changes in the fluorescence signals.

Verification of the helix stabilization by the formation of sandwich complexes between substituents at an $i, i+4$ spacing:

To further verify that the helix formation was indeed induced by metal-ion complexation between substituents at an $i, i+4$ spacing, two kinds of control octamers were designed and synthesized. Their sequences are shown in Figure 7. Each control octamer possessed only four metal-ion chelators on the side chains, whereas the remaining four were replaced with *N*-Boc protecting groups. Category A octamers, comprising of **1,2,5,6-** and **3,4,7,8-OPLM₈**, could produce two sandwich complexes between the i and $i+4$ residues and subsequently fold into a helix with some

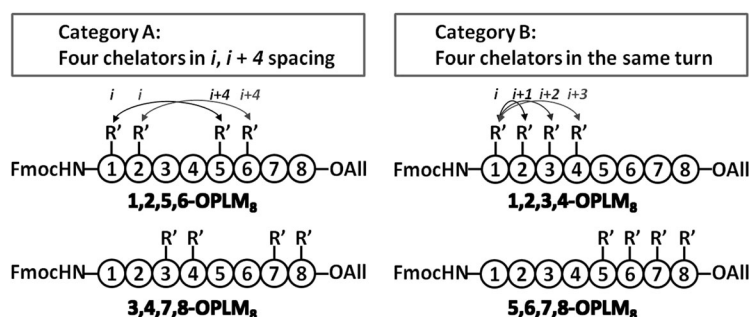


Figure 7. Sequence representations of two categories of control octamers. Category A: four metal-ion chelators are arranged at an $i, i+4$ spacing; Category B: four metal-ion chelators are positioned in the same turn.

stability. Category B octamers, comprising of **1,2,3,4-** and **5,6,7,8-OPLM₈**, with four metal-ion chelators positioned in the same turn, were incapable of forming intramolecular metal complexes at the *i, i+4* positions due to their unfavorable spatial disposition of the chelators. The two categories of control octamers were obtained from the same starting materials (**Boc₂** and **OPLM₂**) by a selective deprotection process and an amide coupling reaction, constructing different sequences (refer to Schemes S3–S5 in the Supporting Information).

The results of absorption, fluorescence emission, and circular dichroism experiments on these four control octamers (see Figures 8 and 9) suggested that **1,2,5,6-** and **3,4,7,8-**

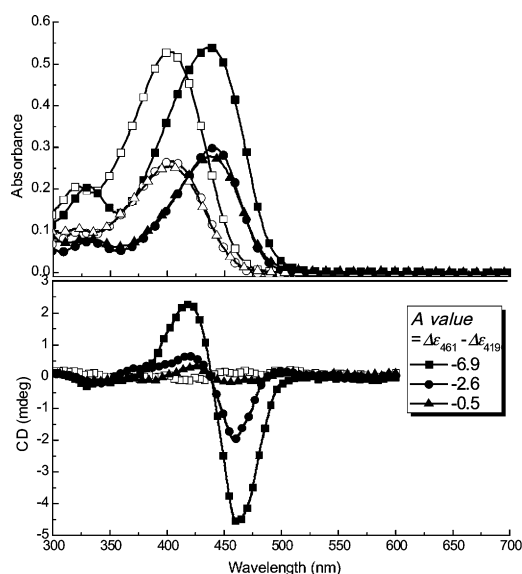


Figure 8. Absorption (top) and circular dichroism (bottom) spectra of **OPLM₈** (■) and control octamers of Category A: **3,4,7,8-OPLM₈** (●) and **1,2,5,6-OPLM₈** (▲) in CH₂Cl₂ (2 × 10⁻⁶ M) in the absence (open symbols) and presence (solid symbols) of 4 equivalents Sr²⁺.

OPLM₈ exhibited similar behavior to **OPLM₈** upon titration with Sr²⁺ (albeit with smaller *A* values), whereas **1,2,3,4-** and **5,6,7,8-OPLM₈** showed completely different folding modes to that of **OPLM₈**. The Sr²⁺-complexed structures of both **1,2,5,6-** and **3,4,7,8-OPLM₈** (Figure 8) revealed a negative Cotton couplet centered around their absorption bands at 438 nm. The *A* value of **3,4,7,8-OPLM₈** was close to half of that of **OPLM₈**. This result was expected as the former contained half the number of metal-ion chelators of the latter. However, **3,4,7,8-OPLM₈** apparently had a better helix-promoting ability than **1,2,5,6-OPLM₈** on the basis of its higher *A* value. The difference in the folding ability may arise from the bulky and long side-chain (metal-ion chelator) on the *N*-terminal α -carbon of **1,2,5,6-OPLM₈**, which did not adopt the adequate geometry to fold as in **3,4,7,8-OPLM₈** (Figure S10 in the Supporting Information).

In the case of the **1,2,3,4-** and **5,6,7,8-OPLM₈** controls of category B, their ICD signals split into negative peaks at 468

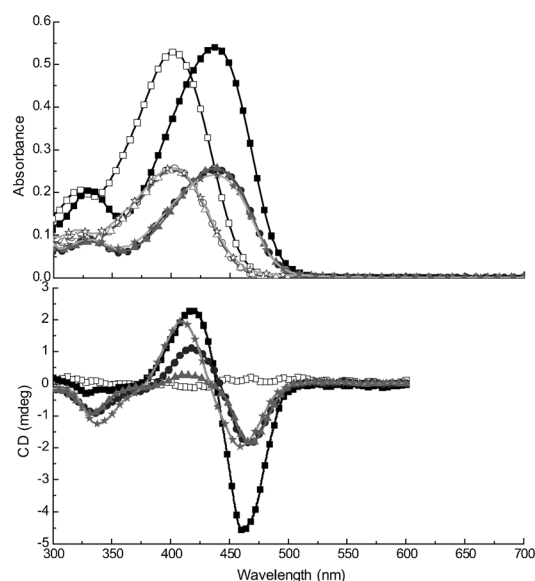


Figure 9. Absorption (top) and circular dichroism (bottom) spectra of **OPLM₈** (■), **OPLM₄** (★), and control octamers of Category B: **1,2,3,4-OPLM₈** (●) and **5,6,7,8-OPLM₈** (▲) in CH₂Cl₂ (2 × 10⁻⁶ M) in the absence (open symbols) and presence (solid symbols) of 2 equivalents Sr²⁺ (in the case of **OPLM₈**, 4 equiv Sr²⁺ were used).

and 334 nm and a positive peak at 418 nm upon the addition of 2 equivalents of Sr²⁺ (Figure 9). The changes in the CD spectra in response to Sr²⁺ were different from those of **OPLM₈**, suggesting that **1,2,3,4-OPLM₈** and **5,6,7,8-OPLM₈** may possibly have formed intrastrand sandwich metal complexes between adjacent chelators because of the flexible lysine side chains. Based on these control results, it can be concluded that the helix formation was indeed induced by the formation of four sandwich complexes between substituents at an *i, i+4* spacing in **OPLM₈**. Notably, **OPLM₄** and **1,2,3,4-OPLM₈** displayed similar absorption changes and ICD signals in the presence of 0.4–2.4 equivalents of Sr²⁺, but different ICD profiles upon the addition of further Sr²⁺ (Figure 9 and Figure S9 in the Supporting Information). These results were not surprising because the complexes share some common structural features, such as four consecutive metal-ion chelators positioned in the same order, although they differ in the peptide length. This observation confirms that the length of a peptide influences the secondary structure to a certain extent.

Kinetics and stability: To assess the kinetics and stability of the alkaline earth metal ion induced helical form of **OPLM₈**, a time-course experiment was carried out by following the ICD signals at 426 and 463 nm after the addition of 4 equivalents of Sr²⁺ (Figure S11 in the Supporting Information). It took only four minutes to reach the plateau of CD enhancement that corresponds to a stable helix conformation at room temperature.^[19] This result clearly indicates that the helical structure promoted by the strong coordination interaction between metal-ion chelators at *i, i+4* spacing and metal ions is formed rapidly and is quite stable.

Conclusion

In summary, our studies outline the structural design of a metal-ion-responsive and fluorescence-detectable foldamer, **OPLM₈**, that is capable of undergoing folding/unfolding transitions upon alkaline earth metal-ion complexation. Even the short L-lysine-based octamer could fold into a stable helical conformation through the coordination interaction between the metal-ion chelators and the alkaline earth metal ions. The metal-ion-induced suprastructural changes in the synthetic foldamer could be easily probed by changes in the fluorescence intensities with concomitant changes in the CD signals. In addition, we have demonstrated that the helix formation is indeed induced by the formation of sandwich complexes between groups at an *i*, *i*+4 spacing through systematic variation of the sequences in a series of control foldamers. The magnitude of the circular dichroism effect showed a linear correlation with the number of sandwich complexes formed.

Experimental Section

General: All chemicals were purchased from commercial sources and were used as received. Solvents for syntheses were dried by standard literature methods before being distilled and stored under nitrogen over 4 Å molecular sieves. ¹H (400 MHz) and ¹³C (100 MHz) NMR spectra were recorded on a Varian Mercury 400 spectrometer. ¹³C (200 MHz) NMR spectra were recorded on a Bruker AVIII 800 MHz spectrometer. Chemical shifts were referenced to selected residual proton peaks of the deuterated solvents and are reported in δ(ppm). ¹H NMR data are reported in the following order: chemical shift, multiplicity (s=singlet, d=doublet, t=triplet, q=quartet, m=multiplet, br=broad), coupling constant(s) in Hertz, number of protons. Melting points were determined on a Fargo MP-1D melting point apparatus without correction. ESI mass spectra were recorded on a Waters Micromass[®] LCT Premier XE system. MALDI-TOF mass spectra were recorded on a Bruker Autoflex III TOF/TOF instrument using 4-hydroxy- α -cyanocinnamic acid (α -CHC) and 2,5-dihydroxybenzoic acid (DHB) as matrices.

Synthesis of compound AcidAC: A 0.5 M aqueous lithium hydroxide solution (5.6 mL) was added to a solution of **EsterAC** (1.43 g, 2.52 mmol) in MeOH (25 mL) and the reaction mixture was stirred for 2 h at reflux. After confirming completion of the reaction by TLC, the reaction mixture was neutralized with acidic resin, filtered, and concentrated to leave a crude solid, which was purified by flash column chromatography on silica gel eluting with CH₂Cl₂/MeOH/acetic acid (9:1:0.01) to give **AcidAC** as an orange solid (1.19 g, 2.14 mmol). Yield 82%; *R*_f=0.14 (CH₂Cl₂/MeOH, 9:1); ¹H NMR (400 MHz, CDCl₃/drops CD₃OD): δ=7.73 (s, 1H), 7.52 (d, *J*=8.8 Hz, 2H), 7.18 (d, *J*=8.8 Hz, 1H), 6.49–6.45 (m, 3H), 6.31 (s, 1H), 3.99 (s, 2H), 3.59–3.58 (m, 4H), 3.47–3.44 (m, 16H), 2.99 ppm (s, 3H); ¹³C NMR (100 MHz, CDCl₃): δ=189.9, 170.9, 160.0, 156.2, 153.2, 151.3, 146.0, 131.9, 129.9, 123.6, 118.4, 110.2, 109.7, 108.0, 97.2, 70.5, 69.7, 69.3, 67.7, 53.5, 52.3, 39.3 ppm; IR (KBr): $\tilde{\nu}$ =1716, 1685 cm⁻¹ (C=O); HRMS (ESI): *m/z* calcd for C₂₉H₃₄N₂O₉: 554.2264; found 577.0837 (*M*+Na⁺).

Synthesis of OPLM₁: DCC (353 mg, 1.74 mmol), HOBt (233 mg, 1.73 mmol), and a catalytic amount of DMAP (23 mg, 0.17 mmol) were added to a solution of **AcidAC** (414 mg, 0.75 mmol) and **N^ε-amino-Boc₁**^[20] (315 mg, 0.77 mmol) in dry CH₂Cl₂ (18 mL) and the reaction mixture was stirred at room temperature for 14 h. After confirming completion of the reaction by TLC, the mixture was filtered through a pad of cotton to remove most of the by-product (*N,N*-dicyclohexylurea). The filtrate was concentrated and purified by flash column chromatography on silica gel eluting with a gradient of CH₂Cl₂/MeOH (from 95:5 to 9:1)

to give **OPLM₁** as an orange solid (468 mg, 0.50 mmol). Yield 67%; m.p. 107–109 °C; *R*_f=0.39 (CH₂Cl₂/MeOH, 95:5); ¹H NMR (400 MHz, CDCl₃/drops CD₃OD): δ=7.76 (s, 1H), 7.74–7.70 (m, 4H), 7.57–7.56 (m, 2H), 7.35 (dd, *J*=8.0, 7.2 Hz, 2H), 7.30–7.25 (m, 3H), 6.72 (t, *J*=5.2 Hz; NH), 6.59 (d, *J*=8.8 Hz, 2H), 6.54 (d, *J*=10.8 Hz, 1H), 6.48 (s, 1H), 5.91–5.81 (m, 1H), 5.60 (d, *J*=8.0 Hz; NH), 5.28 (d, *J*=17.2 Hz, 1H), 5.21 (d, *J*=10.0 Hz, 1H), 4.59 (d, *J*=6.0 Hz, 2H), 4.40–4.36 (dd, *J*=7.6, 7.2 Hz, 1H), 4.33–4.27 (m, 2H), 4.17 (t, *J*=7.2 Hz, 1H), 3.96 (s, 2H), 3.73 (t, *J*=6.0 Hz, 4H), 3.64–3.55 (m, 16H), 3.27–3.22 (m, 2H), 3.09 (s, 3H), 1.70–1.65 (m, 2H), 1.55–1.48 (m, 2H), 1.36–1.26 ppm (m, 2H); ¹³C NMR (100 MHz, CDCl₃): δ=188.6, 171.3, 168.0, 158.9, 155.9, 155.4, 152.5, 151.1, 144.5, 143.2 (×2), 140.6, 131.8, 131.0, 129.6, 127.2, 126.6, 124.6 (×2), 123.7, 120.5, 119.5, 118.4, 110.2, 109.8, 108.7, 98.0, 71.1, 70.1, 69.8, 68.0, 66.8, 65.8, 57.1, 53.9, 52.8, 47.2, 39.9, 39.0, 31.9, 29.1, 22.8 ppm; IR (KBr): $\tilde{\nu}$ =1722, 1677 cm⁻¹ (C=O); HRMS (ESI): *m/z* calcd for C₅₃H₆₀N₄O₁₂: 944.4208; found: 945.4276 (*M*+H⁺).

General procedure for selective deprotection of an allyl group using a Pd⁰ catalyst:^[21] The allyl-protected compound was dissolved in dry DMF under oxygen-free N₂ and then a catalytic amount of [Pd(PPh₃)₄] (10 mol %) and *N*-methylaniline (0.3 mol %) were added. The mixture was stirred at ambient temperature for 8 h. After the reaction was complete, the excess DMF was removed and the crude mixture was purified by centrifugation. The residue was redissolved in a small volume of CH₂Cl₂, precipitated with an eight-fold volume of hexane, and then purified by centrifugation at 5500 rpm for 15 min in a glass tube. The supernatant was removed. The precipitate was redissolved in CH₂Cl₂ and the washing procedure was repeated three times to obtain the pure compound.

General procedure for selective deprotection of an Fmoc group by using 20% piperidine in DMF: The Fmoc-protected compound was dissolved in CH₂Cl₂, and then 20% piperidine in DMF was added. The mixture was stirred at ambient temperature for about 10–20 min (TLC monitoring). The solvents were removed in vacuo and the crude mixture was purified by centrifugation. It should be noted that heating during drying of the crude product causes an unwanted side reaction. The residue was redissolved in a small volume of CH₂Cl₂, precipitated with an eight-fold volume of hexane, and then purified by centrifugation at 5500 rpm for 15 min in a glass tube. The supernatant was removed. The precipitate was redissolved in CH₂Cl₂ and the washing procedure was repeated three times to obtain the pure compound.

General procedure for amide coupling: Amides were prepared from the corresponding carboxylic acids and amines through amide-bond formation. DCC (2.3 equiv), HOBt (2.3 equiv), and a catalytic amount of DMAP (0.24 equiv) were added to a solution of the amine (1.0 equiv) and carboxylic acid (1.02 equiv) in dry CH₂Cl₂. The products became more viscous as the number of repeating units increased. The use of a mixed solvent of CH₂Cl₂/DMF facilitated the coupling reaction and improved the product yield. After confirming completion of the reaction by TLC, the solvents were removed under vacuum and the residue was purified by flash column chromatography on silica gel eluting with different ratios of CH₂Cl₂/MeOH to give the desired compounds.

Synthesis of OPLM₂: Coupling of **OPLM₁-COOH** (340 mg, 0.38 mmol) with **OPLM₁-NH₂** (266 mg, 0.37 mmol) in the presence of DCC (180 mg, 0.87 mmol), HOBt (117 mg, 0.87 mmol), and DMAP (11 mg, 0.09 mmol) gave **OPLM₂** (518 mg, 0.32 mmol) as an orange solid. Yield 87%; m.p. 118–120 °C; *R*_f=0.10 (CH₂Cl₂/MeOH, 95:5); ¹H NMR (400 MHz, CDCl₃/drops CD₃OD): δ=7.75 (s, 1H), 7.71 (s, 1H), 7.66–7.62 (m, 6H), 7.59–7.55 (NH), 7.50–7.48 (m, 2H), 7.41 (m, 2H), 7.34–7.16 (m, 4H), 6.55–6.50 (m, 6H), 6.41 (s, 2H), 6.10 (d, *J*=7.6 Hz; NH), 5.79–5.73 (m, 1H), 5.19 (d, *J*=16.8 Hz, 1H), 5.11 (d, *J*=10.4 Hz, 1H), 4.47–4.42 (br, 3H), 4.20 (d, *J*=7.2 Hz, 2H), 4.14 (m, 1H), 4.07–4.03 (m, 1H), 4.00–3.93 (br, 3H), 3.68–3.50 (br, 40H), 3.26–3.18 (br, 4H), 3.10 (s, 3H), 3.03 (s, 3H), 1.78–1.21 ppm (br, 12H); ¹³C NMR (100 MHz, CDCl₃): δ=189.4, 189.2, 172.0, 171.6, 169.0, 168.6, 159.7, 159.5, 156.3, 155.9, 153.2, 153.1, 151.4, 145.3, 145.0, 143.6, 143.4, 140.9, 132.1, 131.4, 130.0, 129.9, 127.4, 126.9, 126.8, 124.9, 124.0, 119.9, 119.7, 118.4, 110.4, 110.1, 108.6, 108.4, 97.9, 71.1, 70.1, 69.8, 67.9, 66.8, 65.6, 56.8, 56.6, 54.6, 52.8, 52.2, 47.0, 40.3, 40.0, 39.0, 38.4, 32.5, 30.7, 28.9, 28.5, 22.6, 22.3 ppm; IR (KBr): $\tilde{\nu}$ =1720, 1679 cm⁻¹ (C=

O); HRMS (BioTOF II): m/z calcd for $C_{88}H_{104}N_8O_{21}$: 1608.7316; found: 805.8643 ($[M+2H^+]/2$).

Synthesis of OPLM₄: Coupling of OPLM₂-COOH (311 mg, 0.20 mmol) with OPLM₂-NH₂ (262 mg, 0.19 mmol) in the presence of DCC (95 mg, 0.46 mmol), HOBT (13 mg, 0.10 mmol), and DMAP (3 mg, 0.02 mmol) afforded OPLM₄ (341 mg, 0.12 mmol) as an orange solid. Yield 61%; m.p. 173–176 °C; $R_f=0.27$ ($CH_2Cl_2/MeOH$, 9:1); 1H NMR (400 MHz, $CDCl_3$ /drops CD_3OD): $\delta=7.70$ –7.08 (m, 31H), 6.52–6.34 (m, 17H), 5.72–5.65 (m, 1H), 5.13–5.03 (m, 2H), 4.39 (br, 2H), 4.30–4.16 (m, 3H), 4.08–3.83 (m, 12H), 3.69–3.50 (m, 80H), 3.24–3.00 (m, 20H), 1.71–1.23 ppm (m, 24H); ^{13}C NMR (100 MHz, $CDCl_3$): $\delta=189.6$ ($\times 2$), 171.9, 171.4, 169.1 ($\times 3$), 159.8 ($\times 3$), 156.3, 153.2 ($\times 2$), 151.6, 145.3, 143.5, 143.3, 140.8, 132.1, 131.2, 130.0, 127.5, 126.8, 124.8, 124.0, 119.9, 119.6, 118.4, 110.4, 110.1, 108.4 ($\times 2$), 97.8, 71.0, 70.1, 69.8, 68.0, 66.8, 65.7, 56.3, 52.7, 46.9, 39.9, 38.8, 31.9, 31.1, 30.9, 29.6, 28.7, 28.5, 22.6 ppm; IR (KBr): $\tilde{\nu}=1719$, 1667 cm^{-1} (C=O); HRMS (BioTOF II): m/z calcd for $C_{158}H_{192}N_{16}O_{39}$: 2937.3533; found: 980.5125 ($[M+3H^+]/3$).

Synthesis of OPLM₈: Coupling of OPLM₄-COOH (83 mg, 0.03 mmol) with OPLM₄-NH₂ (72 mg, 0.03 mmol) in the presence of DCC (13 mg, 0.06 mmol), HOBT (1.8 mg, 0.01 mmol), and DMAP (0.4 mg, 0.003 mmol) afforded OPLM₈ (102 mg, 0.02 mmol) as a yellowish-orange solid. Yield 70%; m.p. 158–162 °C; 1H NMR (400 MHz, $CDCl_3$ /drops CD_3OD): $\delta=7.74$ –7.13 (m, 56H), 6.56–6.37 (m, 32H), 5.80–5.60 (m, 1H), 5.24–5.08 (m, 2H), 4.44 (br, 2H), 4.39–4.20 (m, 3H), 4.10–3.88 (m, 24H), 3.69–3.56 (m, 160H), 3.43–3.06 (m, 40H), 1.76–1.22 ppm (m, 48H); ^{13}C NMR (200 MHz, $CDCl_3$): $\delta=190.0$ ($\times 3$), 172.9 ($\times 2$), 172.4 ($\times 3$), 171.5 ($\times 2$), 169.4 ($\times 5$), 160.0 ($\times 2$), 156.5 ($\times 2$), 153.5 ($\times 2$), 151.8, 145.6 ($\times 3$), 143.6 ($\times 2$), 141.0, 132.3 ($\times 2$), 130.2, 127.6, 127.0, 125.0 ($\times 2$), 124.2 ($\times 3$), 120.1, 119.8, 110.7 ($\times 2$), 110.2, 108.6 ($\times 3$), 97.8 ($\times 3$), 71.0, 70.1, 69.8, 68.0, 66.8, 66.6, 56.2 ($\times 2$), 55.0, 53.4 ($\times 2$), 52.7, 46.9, 46.4, 39.9 ($\times 3$), 38.8 ($\times 4$), 31.8, 29.5 ($\times 4$), 28.8 ($\times 3$), 22.6 ppm ($\times 4$); IR (KBr): $\tilde{\nu}=1718$, 1666 cm^{-1} (C=O); MALDI-TOF MS (matrix: α -CHC): m/z calcd for $C_{298}H_{368}N_{32}O_{75}$: 5594.5966; found: 5595.702 ($M+H^+$).

Spectroscopic studies: High-throughput fluorescence screening of metal ions was performed using a Wallac 1420 VICTOR² plate reader. All solutions were prepared in either spectroscopic grade CH_3CN or CH_2Cl_2 without special efforts to exclude water or air.

UV/Vis, fluorescence, and circular dichroism titration studies: Absorption spectra were recorded on a Hewlett–Packard 8453A diode-array spectrometer under the control of a Pentium PC running the manufacturer-supplied software package. Fluorescence spectra were obtained on a Hitachi F-4500 spectrometer. CD spectra were recorded on a JASCO J-810 spectropolarimeter using a quartz cell with an optical path length of 1 cm under nitrogen atmosphere. A typical titration experiment was carried out as follows. A solution of the molecule of interest was prepared in spectroscopic grade CH_2Cl_2 (2×10^{-6} M), and a 2 mL portion was transferred to a 1 cm quartz cuvette. A small aliquot of a stock solution of the examined metal ion (1.6 mM) in spectroscopic grade CH_3CN with perchlorate as the counterion was then added. The absorption and fluorescence spectra of the molecule of interest were both recorded as a function of the metal-ion concentration.

Acknowledgements

The authors would like to thank the National Science Council of the Republic of China, Taiwan, and the National Taiwan University for financial support, as well as Dr. S.-J. Huang and Ms. S.-L. Huang at the Instrumentation Center, National Taiwan University, for their assistance with the 800 MHz NMR measurements.

- [1] a) M. W. Pecuh, A. D. Hamilton, *Chem. Rev.* **2000**, *100*, 2479–2494; b) W. E. Stites, *Chem. Rev.* **1997**, *97*, 1233–1250; c) S. Jones, J. M. Thornton, *Proc. Natl. Acad. Sci. USA* **1996**, *93*, 13–20.

- [2] a) E. Yashima, K. Maeda, H. Iida, Y. Furusho, K. Nagai, *Chem. Rev.* **2009**, *109*, 6102–6211; b) B. M. Rosen, C. J. Wilson, D. A. Wilson, M. Peterca, M. R. Imam, V. Percec, *Chem. Rev.* **2009**, *109*, 6275–6540.
- [3] a) H. Juwarker, J.-M. Suk, K.-S. Jeong, *Chem. Soc. Rev.* **2009**, *38*, 3316–3325; b) H. Juwarker, K.-S. Jeong, *Chem. Soc. Rev.* **2010**, *39*, 3664–3674.
- [4] J.-M. Suk, V. R. Naidu, X. Liu, M. S. Lah, K.-S. Jeong, *J. Am. Chem. Soc.* **2011**, *133*, 13938–13941.
- [5] a) R. M. Meudtner, S. Hecht, *Angew. Chem.* **2008**, *120*, 5004–5008; *Angew. Chem. Int. Ed.* **2008**, *47*, 4926–4930; b) Y. Hua, A. H. Flood, *J. Am. Chem. Soc.* **2010**, *132*, 12838–12840.
- [6] D. J. Hill, M. J. Mio, R. B. Prince, T. S. Hughes, J. S. Moore, *Chem. Rev.* **2001**, *101*, 3893–4012.
- [7] M. Yamamura, J. Miyake, Y. Imamura, T. Nabeshima, *Chem. Commun.* **2011**, *47*, 6801–6803.
- [8] a) M. J. I. Andrews, A. B. Tabor, *Tetrahedron* **1999**, *55*, 11711–11743; b) C. E. Schafmeister, J. Po, G. L. Verdine, *J. Am. Chem. Soc.* **2000**, *122*, 5891–5892; c) C. M. Haney, M. T. Loch, W. S. Horne, *Chem. Commun.* **2011**, *47*, 10915–10917.
- [9] C. Dolain, Y. Hatakeyama, T. Sawada, S. Tashiro, M. Fujita, *J. Am. Chem. Soc.* **2010**, *132*, 5564–5565.
- [10] a) C. A. Royer, *Chem. Rev.* **2006**, *106*, 1769–1784; b) X. Michalet, S. Weiss, M. Jäger, *Chem. Rev.* **2006**, *106*, 1785–1813.
- [11] a) Z. Zhong, Y. Zhao, *Org. Lett.* **2007**, *9*, 2891–2894; b) I. J. Lee, B. H. Kim, *Chem. Commun.* **2012**, *48*, 2074–2076.
- [12] C.-T. Chen, W.-P. Huang, *J. Am. Chem. Soc.* **2002**, *124*, 6246–6247.
- [13] N. Solladié, A. Hamel, M. Gross, *Tetrahedron Lett.* **2000**, *41*, 6075–6078.
- [14] OPLM₈ shows good solubility in CH_2Cl_2 , $CHCl_3$, and DMF, but its NMR peaks in these solvents are quite broad and cannot be well resolved owing to a certain degree of aggregation. ^{13}C NMR (200 MHz) spectra of OPLMs were thus recorded on a Bruker AVIII 800 MHz spectrometer to give better resolved carbonyl peaks. The structural identity of OPLM₈ was supported by detection of the correct parent ion peak in the MALDI-TOF mass spectrum with 4-hydroxy- α -cyanocinnamic acid (α -CHC; see the Supporting Information, Figure S1).
- [15] P. D. Beer, A. D. Keefe, H. Sikanyika, C. Blackburn, J. F. McAleer, *J. Chem. Soc. Dalton Trans.* **1990**, 3289–3294.
- [16] In the absence of Sr^{2+} , the low fluorescence intensity was defined as the “OFF” state. At 4 equivalents of Sr^{2+} , the fluorescence intensity increased slightly (about 0.7-fold), but was still defined as the “OFF” state. At 10 equivalents, the fluorescence was enhanced 5-fold, and was defined as the “ON” state.
- [17] a) R. Murugavel, R. Korah, *Inorg. Chem.* **2007**, *46*, 11048–11062; b) L. M. Teesch, J. Adams, *J. Am. Chem. Soc.* **1990**, *112*, 4110–4120.
- [18] OPLM₈ shows good solubility in CH_2Cl_2 , $CHCl_3$, and DMF. However, metal-induced changes in circular dichroism were only observed in CH_2Cl_2 and $CHCl_3$; no such changes were observed in DMF. The UV cut-off of these two solvents is near 240 nm. Thus, it was difficult to determine the backbone structures in these media since the peptide bond absorption was in the far-UV region (180–240 nm).
- [19] The helix that formed in solution was stable for at least 1 h.
- [20] a) S. Wiek, E. Masiukiewicz, B. Rzeszutarska, *Chem. Pharm. Bull.* **1999**, *47*, 1489–1490; b) P. Watts, C. Wiles, S. J. Haswell, E. Pombo-Villar, *Tetrahedron* **2002**, *58*, 5427–5439; c) D. Andreu, S. Ruiz, C. Carreño, J. Alsina, F. Albericio, M. Á. Jiménez, N. de La Figuera, R. Herranz, M. T. García-López, R. González-Muñiz, *J. Am. Chem. Soc.* **1997**, *119*, 10579–10586.
- [21] B. Holm, J. Broddefalk, S. Flodell, E. Wellner, J. Kihlberg, *Tetrahedron* **2000**, *56*, 1579–1586.

Received: August 23, 2012
Published online: November 28, 2012